www.sciencemag.org/content/350/6264/1104/suppl/DC1

Supplementary Materials for

Cotranslational protein folding on the ribosome monitored in real time

Wolf Holtkamp, Goran Kokic, Marcus Jäger, Joerg Mittelstaet, Anton A. Komar, Marina V. Rodnina*

*Corresponding author. E-mail: rodnina@mpibpc.mpg.de

Published 27 November 2015, *Science* **350**, 1104 (2015)
DOI: 10.1126/science.aad0344

This PDF file includes:

Materials and Methods

Cloning of the HemK construct

The gene coding for the protein methyl transferase HemK (ECBD_2409, 834 bp, 277 aa) was amplified from the genomic DNA of *E. coli* BL21 DE3 by colony PCR using the primers 5'-GTCCGAGCAGGACATATGGAATATCAA-3' and 5'-GCAGTGTAG AAAAACCTCGAGTTGATAAT-3', digested with NdeI and XhoI (New England Biolabs) and ligated into a pET-24a Vector (Novagen). The gene sequence encoding for the N-terminal domain of *E. coli* HemK (residues 1-73, HemK NTD hereafter) was amplified by PCR from a vector encoding full-length HemK (residues 1-277), using primers containing recognition sequences for NdeI and XhoI restriction enzymes for subsequent cloning into expression vector pET24-a (Novagen). The purified PCR fragment was digested with NdeI and XhoI restriction enzymes for 1 h and ligated into the expression vector pET-24a linearized with the same restriction enzymes. The Leu-Glu sequence (encoded by the XhoI restriction used for cloning) was subsequently removed by inverse deletion PCR. Mutants of wild type NTD-HemK were made by PCR using a commercial site-directed mutagenesis kit (Stratagene, Carlsbad, CA) according to the manufacturer's instructions. We note that HemK from *E. coli* BL21 DE3 contains Lys at position 34, in contrast to HemK from *E. coli* K12, which contains Arg at position 34 and the structure of which is available. In the following, the sequence of HemK from *E. coli* BL21 DE3 is denoted as wild type (wt). Endogenous tryptophan residues at position 6 and 78 were replaced with phenylalanine in all constructs using the quick-change method. For PET experiments tryptophan residues were introduced at position 6, 38, and 49 using site-directed mutagenesis. All constructs were verified by sequencing.

Expression and purification of HemK NTD

The plasmid encoding HemK NTD (or its mutants) was transformed into competent *E. coli* BL21 DE3 cells (Novagen). Protein expression was carried out in LB medium supplemented with 50 µg/ml kanamycin at 37 °C. Overexpression of the HemK NTD was induced at OD600 = 0.6 by the addition of isopropyl-β-D-thiogalactopyranoside (IPTG) to a final concentration of 500 µM. After 3 h induction at 37 °C, bacteria were harvested by centrifugation (5000 rpm, 30 min), the pellet was transferred to a 50 ml Falcon tube, flash frozen in liquid nitrogen and stored at -80 °C until further use.

Purification of overexpressed HemK NTD was performed at 4 °C. Cells were resuspended in buffer A (100 mM Tris, pH 8.0, 700 mM NaCl, 1 mM DTT, supplemented with 0.5 mg/ml bovine DNAse and Roche protease inhibitor cocktail) and sonified on ice (10 x 30 s sonification intervals, with 2 min cooling intervals to minimize overheating of the solution). The lysed bacteria were centrifuged (15,000 g, 45 min). The supernatant was passed through a 0.45 micron filter membrane, and loaded onto a Protino 2000 immobilized Ni-chelate affinity column (Macherey Nagel, Düren, Germany), equilibrated in buffer B (buffer A without DNase, protease inhibitor and DTT). The Ni-chelate resin was extensively washed with buffer B until no significant absorption was detectable in the flow-through ($A_{280} < 0.05$). Resin-bound protein was eluted in 5 ml of buffer C (buffer B, 300 mM imidazole). The eluted protein solution was immediately supplemented with 1 mM DTT to prevent oxidation of the Cys (Cys57) and extensively dialyzed (2 x 5 liter) against buffer D (20 mM Tris, pH 8.0, 1 mM DTT). The dialyzed protein solution was injected onto a Q-Sepharose column (GE Healthcare), equilibrated in buffer D. After extensive washing of the column with buffer D (20 column volumes), bound HemK NTD was eluted from the Q-Sepharose resin using a linear salt gradient (0 – 800 mM sodium chloride in buffer D over 40 column volumes, flow rate 5 ml/min). The HemK NTD eluted in a symmetric peak at a NaCl concentration of 150-200 mM. Fractions containing eluted protein were pooled, concentrated to ~ 100 µM

(Centricon, 3 MWCO), extensively dialyzed against buffer E (50 mM MOPS, pH 7.0, 1 mM DTT) and stored in flash-frozen 1 ml aliquots at -80 °C until further use. Protein purity and identity was routinely checked by reversed-phase HPLC and MALDI mass spectrometry, respectively. Protein concentrations were determined spectrophotometrically using a molar extinction coefficient ε_{280} = 7000 cm^{-1} M^{-1} for HemK NTD.

Fluorescence emission spectra and equilibrium chemical unfolding

Fluorescence emission spectra were recorded at 25 °C with a Horiba model Fluorolog 3 spectrofluorimeter connected to a circulating water bath. Measurements were performed in a quartz cuvette of 1-cm path length at a protein concentration of 2 µM in buffer E. Fluorescence was excited at 280 nm. Fluorescence emission spectra were collected between 310 and 420 nm in 1 nm increments and were corrected for background (buffer without protein). Slid widths of 1 and 10 nm were used for excitation and emission, respectively.

Chemical denaturation experiments were performed at 25 °C by preparing 40 solutions of protein containing increasing amounts of urea (0 – 8 M urea in buffer E). The urea stock solution was prepared freshly before each experiment. The molar concentration of the urea stock solution was determined at 25 °C from the difference in the refractive index (ΔN) between the buffered urea stock solution and the buffer solution without denaturant (eq. 1):

$$[\text{urea}]\ (\text{M}) = 117.66(\Delta N) + 29.75(\Delta N)^2 + 185.56(\Delta N)^3 \qquad \text{(eq. 1)}$$

Samples were incubated for 2 hours before measurements were taken. For each collected background-corrected fluorescence emission spectrum, the normalized global emission fluorescence maximum (GF) was calculated (eq. 2):

$$GF\ (\text{nm}) = \Sigma\ (\lambda_i \cdot F_i)/\ \Sigma F_i \qquad \text{(eq. 2)}$$

where $\Sigma\ (\lambda_i \cdot F_i)$ is the wavelength-weighted integrated fluorescence, and ΣF_i is the integrated fluorescence, both calculated from 310-420 nm. A protein denaturation curve was rendered by

plotting the change in global fluorescence against the denaturant concentration. Thermodynamic parameters of folding were extracted by least-squares fitting the sigmoidal denaturation curve with a 6-parameter, apparent two-state equilibrium unfolding model (eq. 3) (*23*), using the GraphPad Prism software package (GraphPad Software Inc, La Jolla, CA):

$$S_{obs}=((S_N \cdot m_N \cdot [D])+(S_D+m_D \cdot [D]) \cdot \exp(-(\Delta G_{ND}-m_G \cdot [D]/RT))/(1+\exp(-(\Delta G_{ND}-m_G \cdot [D])/RT)) \quad (3)$$

where S_{obs} is the observed global fluorescence at urea concentration [D]; S_N, S_D, m_N and m_D represent intercepts and slopes of native and denatured baselines, respectively; m_G is a cooperativity parameter related to the change in exposure of hydrophobic surface area upon unfolding; R is the gas constant, T the absolute temperature (in K) and ΔG_{ND} the unfolding free energy in the absence of denaturant (in kJ/mol). The unfolding transition was normalized to the fraction of folded protein, F_D, using eq. 4:

$$F_N = ((S_N + m_N \cdot [D])-S_{obs})/((S_N + m_N \cdot [D])-(S_D + m_D \cdot [D])) \quad (4)$$

Kinetics of unfolding and refolding

Kinetic unfolding and refolding experiments were performed with an Applied Photophysics SX.17MV stopped-flow fluorimeter (Applied Photophysics, Leatherhead, UK), operated in single-step mixing mode at 25 °C monitoring the fluorescence change of the single Trp residue in HemK. The excitation wavelength was 280 nm (slid width of 2 nm). A 295 nm cut-off glass filter was placed on the emission channel to reject scattered light and to collect emitted light above 295 nm from a cuvette of 2 mm path length. Refolding experiments were performed by a 1:10 dilution of unfolded protein (in buffer E with 5.5 M urea) into solutions containing urea at concentrations in the range of 0-4.5 M (in buffer E), while unfolding experiments were performed by a 1:10 dilution of folded protein (in buffer E) into solutions containing urea in the range of 4.2 – 8.8 M (in buffer E). Unfolding and refolding experiments were performed between 5 and 7 times at each condition, and the average trace was used for

kinetic analysis. Unfolding reactions obeyed single-exponential kinetics, while refolding reactions where biphasic. About 80-85% of the total fluorescence intensity change occurred in the fast refolding phase on the millisecond time scale, while the remaining fluorescence change occurred on the second time scale. HemK NTD contains two Pro residues that adopt a *trans*-conformation in the folded protein. The slower refolding phase may result from slow *cis/trans*-isomerization of a small fraction of denatured protein with either Pro residue adopting the energetically less-favored *cis*-conformation. The kinetic refolding traces were fitted to a double-exponential function, but only the rate constant of the fast phase (originating from molecules with the two Pro residues in their native *trans*-conformation) was considered for further analysis. To determine the microscopic rate constants for folding and unfolding in the absence of denaturant, we plotted the natural logarithm of the apparent (observed) rate constants k_{obs} (determined from exponential fits of the raw unfolding and refolding fluorescence traces) against the denaturant concentration [D] and least-squares fitted the resulting V-shaped curve to a four-parameter kinetic two-state folding model (eq. 5):

$$\ln(k_{obs}) = \ln(k_{f0} \cdot \exp(m_f \cdot [D]/RT) + k_{u0} \cdot \exp(m_u \cdot [D]/RT) \qquad \text{(eq. 5)}$$

where k_{obs} is the apparent, first-order rate constant at denaturant concentration [D], k_{f0} and k_{u0} are the microscopic rate constants of folding and unfolding in the absence of denaturant, and m_f and m_u are constants that describe how much the folding and unfolding rates vary with [D].

Circular dichroism spectroscopy and thermal denaturation experiments

Circular dichroism (CD) spectra and thermal unfolding transitions were recorded with a Chirascan model dichrometer (Applied Photophysics, Leatherhead, UK). Far- and near-UV CD spectra were recorded in buffer E that is transparent enough to collect high quality data down to the 190 nm wavelength range. Thermal unfolding transitions (monitored at 222 nm) were collected in buffer E or buffer I with 1 mM DTT.

Far-UV CD-spectra were recorded from 190-250 nm in 1 nm increments, using a quartz cuvette of 1 mm pathlength and protein solutions at a concentration of 20 µM. The machine unit ellipticity, θ, at each wavelength increment was averaged for 5 s. Three individual far-UV CD spectra were recorded and averaged. The averaged spectra were corrected for background (buffer without protein) and are represented as mean residue molar ellipticities Θ_{MRE}, to allow for the direct comparison of the spectra of wt HemK NTD (and mutants thereof) with the spectrum of the C-terminally truncated fragment of HemK NTD (residues 1-35). Mean residue molar ellipticities (units of $deg \cdot cm^2 \cdot dmol^{-1}$) were calculated from the background-corrected raw machine units of ellipticity θ (units of deg) as follows (eq. 6):

$$\Theta_{MRE}\ (deg \cdot cm^2 \cdot dmol^{-1}) = \theta(mdeg) \cdot 10^6 / (\text{pathlength (mm)} \cdot [\text{protein}]\ (\mu M) \cdot n) \quad \text{(eq. 6)}$$

where path length is the optical path length of the cuvette, and n the number of the absorbing units in the protein (here, the number of peptide bonds in HemK NTD).

Near-UV CD-spectra were collected between 250 and 320 nm at 1-nm increments in quartz cuvettes with a pathlength of 10 mm, using protein solutions at a concentration of 120 µM. At each wavelength increment, the machine unit ellipticity θ was averaged for 30 s. Five individual near-UV CD-spectra were recorded and averaged. Because of the much smaller number of near-UV CD-active chromophores (two Phe, one Tyr, one Trp), background-corrected near-UV CD spectra are represented as molar ellipticities, θ_{ME}, rather than Θ_{MRE}:

$$\Theta_{ME}\ (deg \cdot cm^2 \cdot dmol^{-1}) = \theta(mdeg) \cdot 10^6 / (\text{pathlength (mm)} \cdot [\text{protein}]\ (\mu M)) \quad \text{(eq. 7)}$$

Thermal denaturation experiments were collected in single-wavelength mode (222 nm) from 10 °C to 90 °C in 2 °C increments using a quartz cuvette of 1 mm pathlength and protein solutions at a concentration of 20 µM. The temperature was measured directly in the cuvette using a Peltier thermoelement. At each temperature increment, the machine unit ellipticity Θ was averaged for 40 s after an incubation time of 60 s at the target temperature. Thermal unfolding transitions measured in low-salt buffer E showed a sigmoidal temperature

dependence and were fully reversible. The midpoint of thermal melting (T at which $\Delta G(T) = 0$) measured in buffer 1 with 1 mM DTT exceeded that measured in low-salt buffer E by 1-2 °C. The slight dependence in protein thermal stability on buffer conditions may be attributed to the fact that Tris-based translation buffer is particularly unsuited for thermal denaturation experiments, due to the strong temperature dependence of the pK_a of Tris. All CD experiments reported in the main text were thus collected in buffer E.

Components of translation assay

Ribosomes from *E. coli* MRE 600, initiation factors, EF-G and EF-Tu were prepared as described (*24-27*). To prepare aminoacyl-tRNA (aa-tRNA) containing all amino acids for translation, total tRNA from *E. coli* MRE 600 (Roche) was extracted with phenol and precipitated twice with ethanol. Aminoacylation of total tRNA (80 unit A_{260}/ml) was performed in buffer F (50 mM Hepes-KOH pH 7.5, 70 mM NH_4Cl, 30 mM KCl, 20 mM $MgCl_2$) supplemented with ATP (3 mM), DTT (2 mM), and L-amino acids (Sigma, 300 µM each), using S100 extract (3 % (v/v)) for 1 h at 37°C. Potassium acetate (pH 5, 0.2 M) was added to stop the reaction. The reaction mixture was phenol-extracted (Phenol pH 4.5, Roth) and precipitated twice with ethanol. The tRNA was dissolved in water and purified by FPLC on a HiTrap Q HP column (GE Healthcare). The tRNA was eluted with a linear gradient from 0 M to 1.1 M NaCl in buffer G (50 mM sodium acetate, pH 4.5, and 10 mM $MgCl_2$). The tRNA-containing fractions were pooled, ethanol-precipitated, dried, dissolved in water and stored in aliquots at -80 °C. Total tRNA lacking Lys-$tRNA^{Lys}$ was prepared in the same way, except for omission of Lys in the aminoacylation reaction. f[^{3}H]Met-$tRNA^{fMet}$, BOF-[^{3}H]Met-$tRNA^{fMet}$ and BOP-[^{14}C]Lys-$tRNA^{Lys}$ were was prepared as described (*26, 28*).

Transcription templates for mRNAs of different lengths (coding for the N-terminal portions of HemK of 42, 56, 70, 84, 98, 112, 154 amino acids length) were generated by PCR amplification of the respective construct using the T7 promotor as an upstream primer and

various lower primers annealing at distinct sites in the coding region of HemK. Transcription was carried out in buffer H (40 mM Tris-HCl, pH 7.5, 15 mM $MgCl_2$, 2 mM spermidine, 10 mM NaCl, 10 mM DTT, 3 mM NTPs (each), 5 mM GMP, DNA template (10% (v/v), pyrophosphatase (5 u/ml), RiboLock RNase inhibitor (1.5 % (v/v), Fermentas), and T7 RNA-polymerase (0.8 % (v/v)), for 3h at 37°C. To purify the mRNA from the reaction mixture, the RNeasy kit (Qiagen) was used according to the manufacturer's protocol. The homogeneity of mRNAs (> 95%) was determined by polyacrylamide gel electrophoresis.

In-vitro translation

Initiation complexes were formed in buffer I (50 mM Tris-HCl, pH 7.5, 70 mM NH_4Cl, 30 mM KCl, and 7 mM $MgCl_2$) supplemented with DTT (2 mM) and GTP (2 mM) by incubating 70S ribosomes (1.5 μM), initiation factors IF1, 2 and 3 (2.25 μM each), mRNA (3 μM), and f[^{3}H]Met-tRNA^{fMet} or BOF-[^{3}H]Met-tRNA^{fMet} or f[^{35}S]Met-tRNA^{fMet} (1 μM) for 30 min at 37°C. The final concentration of initiation complexes was determined by nitrocellulose filtration and ^{3}H-radioactivity counting. EF-Tu–GTP complexes were prepared by incubating EF-Tu–GDP (150 μM) with GTP (2 mM) and EF-Ts (0.02 μM) in buffer I supplemented with phosphoenol pyruvate (PEP; 3 mM), pyruvate kinase (0.05 mg/mL), $MgCl_2$ (2 mM) and DTT (2 mM) for 15 min at 37°C. EF-Tu–GTP–aa-tRNA ternary complexes were formed by mixing EF-Tu–GTP with total tRNA (lacking Lys-tRNA^{Lys}) (30 μM) and BOP-[^{14}C]Lys-tRNA^{Lys} (0.2 μM) or [^{14}C]Lys-tRNA^{Lys} (0.2 μM) in translation buffer J (HiFi, 50 mM Tris-HCl, pH 7.5, 70 mM NH_4Cl, 30 mM KCl, 3.5 mM $MgCl_2$, 0.5 mM spermidine, 8 mM putrescine, and 2 mM DTT), followed by incubation for 1 min at 37ºC. Initiation complexes (20 nM), ternary complexes (15 μM) and EF-G (2 μM) were warmed up to 37°C for 1 min and rapidly mixed in buffer J containing GTP (0.5 mM), PEP (1.5 mM), and pyruvate kinase (0.05 μg/μl) to start *in-vitro* translation. The reaction was stopped by flash-freezing in liquid nitrogen, followed by RNase A (0.33 mg/mL, Fermentas) digestion for 30 min at 37°C and incubation in loading

buffer K (50 mM Tris-HCl, pH 6.8, 4% SDS, 2% 2-mercaptoethanol and 12% (w/v) glycerol) for 30 min at room temperature. Translation products were separated on Tris-Tricine SDS-PAGE (*24, 26*) using a 4% stacking, 10% spacer and 16.5% separating gel (49.5% T, 3% C) and visualized on a FLA-9000 fluorescent gel scanner with two lasers set to excitation wavelengths of 488 and 532 nm for BOF and BOP, respectively. Translation products labeled with [^{35}S]Met were visualized by exposing the gel on a phosphor imager screen and scanning on a FLA-7000 phosphor imager. Average rate of protein synthesis was calculated by global fitting of translation time courses obtained for all constructs assuming a linear model with n irreversible steps, where n corresponds to the chain lengths, and a single (average) elemental rate constant of translation per second (amino acids/s). Calculations were carried out with Scientist for Windows software.

Following translation by stopped-flow

Fluorescence experiments were carried out in buffer J (HiFi) containing GTP (0.5 mM), PEP (1.5 mM) and pyruvate kinase (0.05 µg/µl) at 37°C in the SX-20MV stopped-flow apparatus (Applied Photophysics). Equal volumes of initiation complex and ternary complexes containing total aa-tRNA with native Lys-tRNA^{Lys} or BOP-Lys-tRNA^{Lys} at the same concentrations as used in *in-vitro* translation were rapidly mixed. BOF and BOP fluorescence was monitored in parallel upon excitation at 470 nm after passing through 500 nm or 590 nm cut-off filters, respectively. All fluorescence traces were first corrected by subtracting the respective buffer blanks (fig. S4A). Further correction of fluorescence measured in the donor and acceptor channels when both donor and acceptor were present was carried out by subtracting the fluorescence due to the bleed-through of the acceptor in the donor channel ($F_{DA(D)} - F_{A(D)}$) and the bleed-through of donor fluorescence and acceptor in the acceptor channel ($F_{DA(A)} - F_{D(A)}$). The FRET time course for BOF was obtained by subtracting the $F_{D(D)}$ from ($F_{DA(D)} - F_{A(D)}$). Measurements of BOP fluorescence change upon direct excitation of

BOP at 545 nm suggested that the acceptor alone, in the absence of the donor, showed very little fluorescence change while moving through exit tunnel of the ribosome (fig. S4B). FRET efficiencies were calculated according to the equations $FRET=F_{DA}/F_D$, using the corrected F_{DA} values for the donor and acceptor, respectively. The change in FRET after the release of the polypeptide from HemK70-RNCs was monitored after rapidly mixing the RNCs with Pmn (1 mM). To detect PET between the N-terminal BOF and Trp residues in the polypeptide chain, BOF fluorescence was excited at 470 nm and detected after passing a KV500 cut-off filter (Schott). The change in PET after the release of the polypeptide from HemK70-RNCs or HemK112-RNCs was monitored after rapidly mixing the RNCs with Pmn (1 mM). Fluorescence traces in the absence of Trp were subtracted from traces where Trp was present (6W, F39W, D49W) to obtain time-resolved PET efficiencies independent of the intrinsic BOF changes in the peptide exit tunnel (fig. S10).

Limited proteolysis

Ribosome-bound HemK nascent chain complexes were formed by *in vitro* translation, as described above. To monitor the digestion of released peptides, samples were incubated with Pmn (1 mM) for 1 min at 37°C prior to digestion. Proteolysis was started by adding thermolysin (18 ng/µl). The reaction was quenched by adding loading buffer K (50 mM Tris-HCl, pH 6.8, 4% SDS, 2% 2-mercaptoethanol and 12% (w/v) glycerol) and incubated for 10 min at 80°C. Time courses of digestion were analyzed by Tris-Tricine SDS-PAGE and fluorescence scanning of BOF fluorescence in a FLA-9000 fluorescent gel scanner. Images were analyzed with ImageJ software. Time courses of digestion were fitted to single-exponential functions. The stability of nascent wt chains relative to mutant nascent chains was calculated as the ratio between the digestion half-lives (τ) of the native (τ_{wt}) and 4xA (τ_{4xA}) polypeptides of the corresponding lengths.

Supplementary Figures

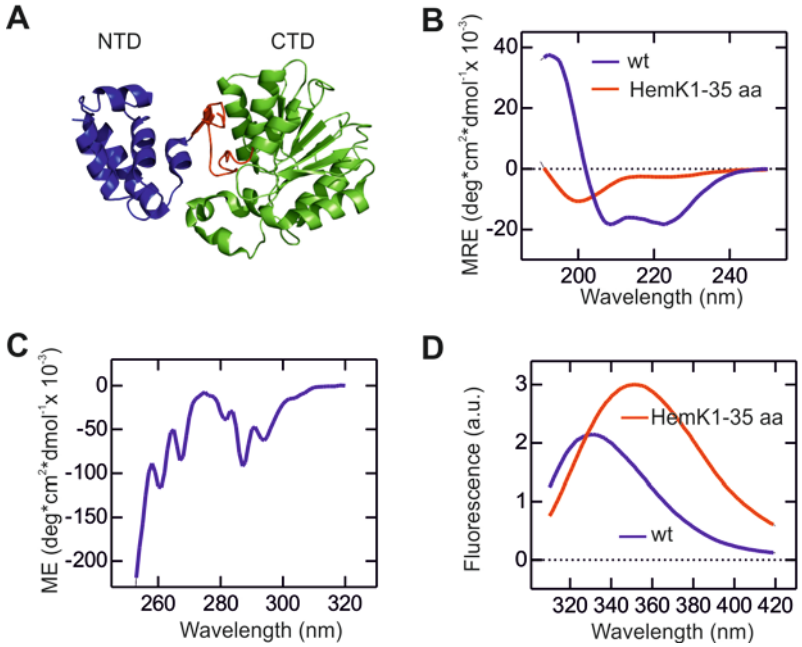

fig. S1.

Related to Fig. 1. The N-terminal domain of *E. coli* HemK folds in isolation.

(A) Two-domain architecture of *E. coli* HemK, a 277-residue protein (N5)-glutamine methyltransferase (PDB ID: 1T43). The N-terminal domain (residues 1-73, color-coded blue, HemK NTD hereafter) folds into a 5-helix-bundle structure that is connected to the C-terminal domain (residues 87-277, color-coded green) via a short β-hairpin linker (color-coded red). The linker-hairpin forms one salt bridge with the NTD (Arg22-Glu75), but there is no direct interaction between the N- and C-terminal domains, suggesting that the HemK NTD folds in isolation.

(B) Far-UV CD spectrum of HemK NTD (blue) and of the C-terminally truncated variant that lacks helices 3-5 (residues 1-35, red) at 25 °C. Double minima at 222 and 208 nm, and a pronounced maximum at 194 nm suggest a high content of α-helix in HemK NTD, consistent

with the crystal structure. The far-UV CD spectrum of HemK 1-35 resembles that of a random coil (single minimum at 200 nm)

(C) Near-UV CD spectrum of HemK NTD at 25 °C. The fine-structure of the spectrum indicates that the aromatic chromophores (side chains of Tyr3, Trp6, Phe38 and Phe42) are in a chiral environment, suggesting a rigid tertiary structure. The two prominent narrow bands at 262 and 268 nm can be attributed to vibrational transitions in the excited state of the Phe side chains. The two red-shifted bands at 287 and 292 nm are typical for an in-plane L1b electronic transition in the indole moiety of Trp6.

(D) Trp-fluorescence emission spectrum of HemK NTD at 25°C. The blue-shifted emission maximum indicates that Trp6 is in a rather apolar environment, consistent with the X-ray structure of full-length HemK NTD that reveals that Trp6 is partially solvent-excluded. The red-shifted fluorescence emission maximum (351 nm) of HemK 1-35 suggests that Trp6 is fully solvent-exposed. While the data shown in (B)-(D) suggest that HemK NTD is fully folded at ambient temperature, the C-terminally truncated variant (residues 1-35) that lacks helices 3-5 appears to be unstructured.

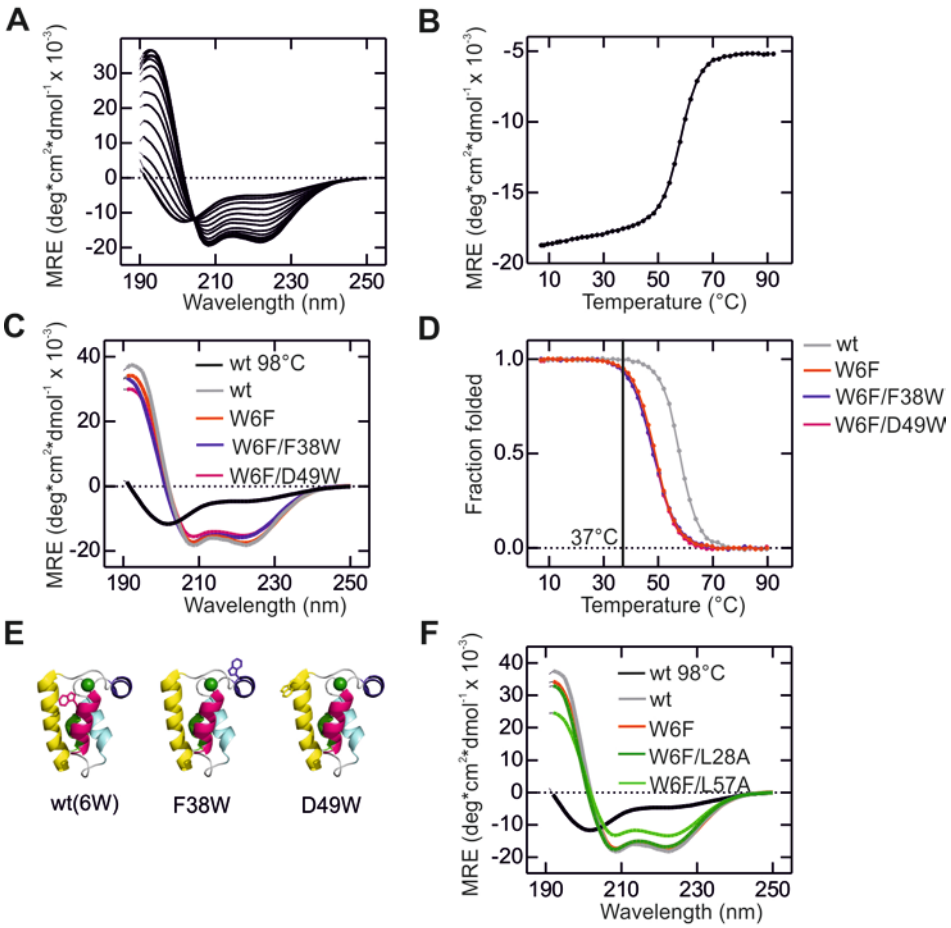

fig. S2.

Related to Fig. 1 and 3. Thermal unfolding and thermal stability of wt and mutant HemK NTD.

(A) Equilibrium thermal unfolding of wt HemK NTD. Shown are representative far-UV CD spectra recorded at temperatures below (< 40 °C), within, and above (> 70 °C) the thermal unfolding transition. The isosbestic point at 204 nm is a strong indicator for a two-state thermal unfolding transition with no folding intermediates populated significantly, and thus supports the conclusions from isothermal urea denaturation experiments (see fig. S3 for details). The far-UV CD spectrum of thermally denatured HemK NTD (80 °C, top-most spectrum) resembles the random-coil-like spectrum of the C-terminally truncated domain (residues 1-35) that is unfolded at ambient temperature (fig. S1B, red curve).

(B) Equilibrium thermal unfolding transition of wt HemK NTD, monitored by far-UV CD at 222 nm. Unfolding is sigmoidal, and the midpoint of thermal unfolding is ~ 57 °C. The thermal transitions were not analyzed thermodynamically (which would require knowledge of the heat capacity). The solid line connecting the data points is thus a visual guide.

(C) Far-UV CD spectra (10 °C) of the three Trp-variants of HemK NTD that were utilized in the co-translational PET experiments (W6F, W6F-F38W, W6F-D49W). The minor differences in spectral shape may be attributed to small conformational changes induced by the mutations, while the variation in spectral intensity may result from small context-dependent contributions of the indole side chain to the far-UV CD spectrum, or, for the variant that lacks a Trp residue, errors in the determination of the protein concentration.

(D) Equilibrium thermal unfolding transitions of the mutants shown in panel c, rendered as the fraction of unfolded protein as a function of temperature. Mutants W6F, W6F-F38W and W6F-D49W are all destabilized relative to wild type, but are >90% folded under conditions where the co-translational folding experiments were performed (37 °C).

(E) Structural cartoon of the three HemK NTD PET-mutants, showing the approximate position of the N-terminal BOF fluorophore (green sphere) and the position of the quencher (Trp).

(F) Far-UV CD spectra (10 °C) of the HemK NTD variants with single Leu to Ala exchanges in the hydrophobic core. The proteins with single mutations are more than 70% unfolded at 37°C (Fig. 3B), but adopt a native-like conformation at low temperature.

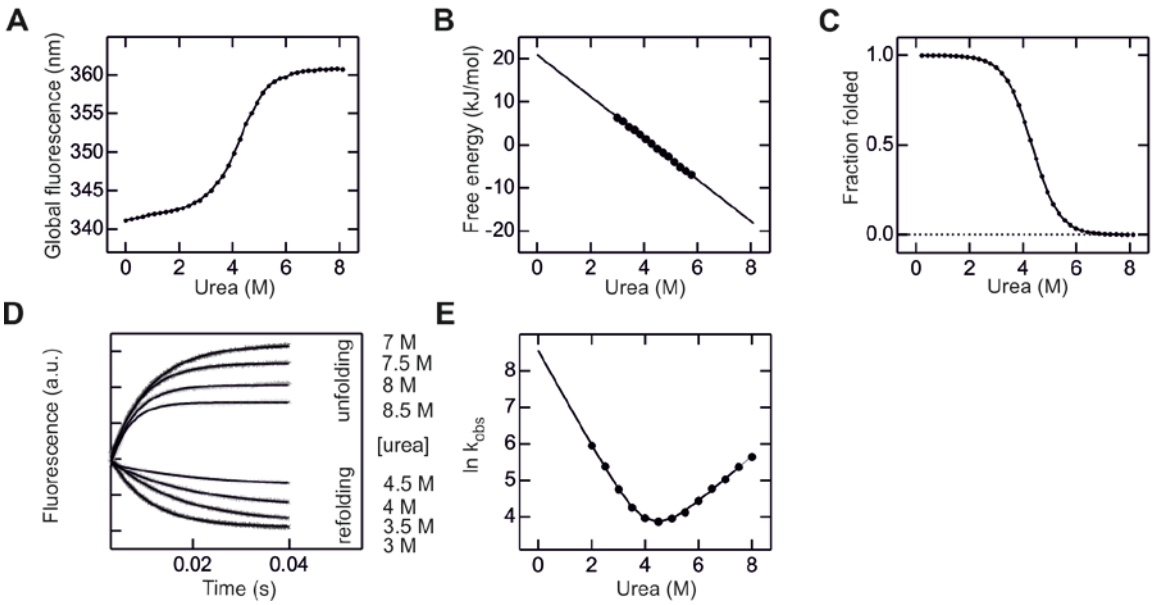

fig. S3.

Related to Fig. 1. Folding thermodynamics and kinetics of HemK NTD.

(A) Urea-induced equilibrium unfolding of HemK NTD at 25°C. The curve displays the change in the global fluorescence emission maximum (eq. 2, Supplementary Materials and Methods) of the Trp-fluorescence emission spectrum as a function of urea concentration. The solid line is a least-square fit of the raw data to a 6-parameter thermodynamic two-state unfolding model (eq. 3, Supplementary Materials and Methods).

(B) Change in the free energy of folding as a function of urea concentration ($\Delta G[Urea] = \Delta G(0M\ urea) - mG[urea]$). The plot was rendered using the thermodynamic parameters ($\Delta G(0M\ urea)$ and mG) obtained from the two-state fit of the raw data. The solid line is an extrapolation of the folding free energies to solution conditions outside the folding transition region. The folding free energy in the absence of denaturant is 20.8 ± 0.4 kJ/mol, whereas the midpoint of folding ([D1/2], with $\Delta G[D1/2)] = 0$) is 4.3 ± 0.1 M urea.

(C) Normalized equilibrium unfolding transition of HemK NTD, showing the fraction of folded protein at each urea concentration. The curve was rendered from the fit of the raw data (panel a) and eq. 4 (Supplementary Materials and Methods).

(D,E) Urea-dependence of the folding and unfolding kinetics of HemK NTD. (D), Time courses of unfolding and refolding at different urea concentrations. (E) The natural logarithm of the observed rate constants (lnk_{obs}) under folding (< 4.3 M urea) and unfolding conditions (> 4.3 M urea) plotted as a function of urea concentration. The continuous line is the best fit of the data to eq. 5 (Supplementary Materials and Methods), which describes a kinetic two-state transition. The extrapolated folding rate constant in aqueous buffer without denaturant (lnk_f ~ 8.5) suggests that HemK NTD folds on the sub-millisecond time scale (folding relaxation time ~ 200 μs at 25°C). A summary of all relevant thermodynamic parameters is provided in table S1. We note that there is excellent agreement in the free energies of folding calculated from equilibrium unfolding experiments and from the microscopic rate constants of folding (k_f) and unfolding (k_{uf}) determined from the kinetic experiments. This supports the validity of a simple two-state folding process. We, however, note that, because of the fast intrinsic folding of HemK NTD, folding rates could only be experimentally determined at [urea] > 2 M. We can therefore not rule out that a transiently formed folding intermediate populates under more stabilizing folding conditions. The presence of such a transiently-populated folding intermediate would be apparent by a small downward curvature (“kinetic roll-over”) in the “refolding-arm” of the V-shaped rate vs. [Urea] plot at low denaturant concentrations. An unambiguous answer to whether a folding intermediate is indeed populated during HemK NTD folding is beyond the scope of this study and has to await more detailed continuous-flow mixing experiments with higher time resolution.

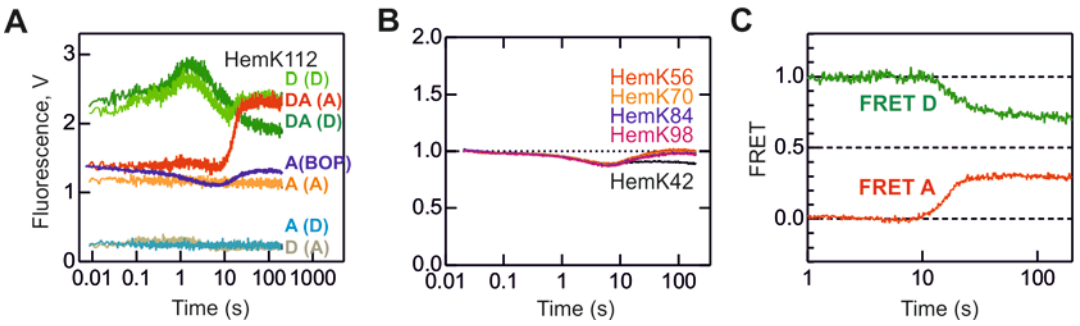

fig. S4.

Related to Fig. 2. Rearrangement from the compact to native-like fold followed by FRET.

(A) Rapid fluorescence changes measured in the donor channel when both donor (BOF) and acceptor (BOP) were present (DA (D); dark green), donor alone (D (D); light green), or acceptor alone (A (D); blue), or in the acceptor channel when both donor and acceptor were present (DA (A); red), donor alone (D (A); olive), acceptor alone (A (A); orange), or when the acceptor was excited directly (A (BOP); dark blue). Each trace was corrected by subtracting the respective buffer signals measured in the donor and acceptor channel, respectively.

(B) Transient fluorescence changes of BOP at position 34 upon translation of HemK constructs as indicated. BOP fluorescence was excited directly in the absence of the BOF donor.

(C) Time-resolved FRET changes of the donor and acceptor calculated from the corrected time courses shown in panel A. FRET efficiency = F(AD)/F(D) for the donor (green) and acceptor (red), respectively. F(AD) for BOF (donor) was calculated as DA(D)-A(D). F(DA) for BOP (acceptor) was calculated as DA(A)-A(A)-D(A)+buffer(A). F(D) is D(D), fluorescence of donor alone in the D channel corrected for the respective buffer blank. The calculated end level FRET efficiency, 0.32, is an apparent value which does not take into account the efficiency of donor incorporation into peptides (about 0.7 of BOF-Met-

$tRNA^{fMet}$ added into the reaction mixture) and the portion of nascent chains containing acceptor BOP-Lys (0.7); the latter values were determined by TCA precipitation of the peptides containing BOF-[^{3}H]Met and BOP-[^{14}C]Lys. When corrected for the donor and acceptor incorporation, the estimated FRET efficiency in folded HemK112 is closer to 0.32/0.7/0.7 = 0.65. Taking into account the relative uncertainty of such calculation and the high fluorescence anisotropy of dyes in nascent chains inside the peptide tunnel (fig. S6B;C), we refrained from calculating distances from FRET and discuss the FRET efficiencies in a qualitative way only.

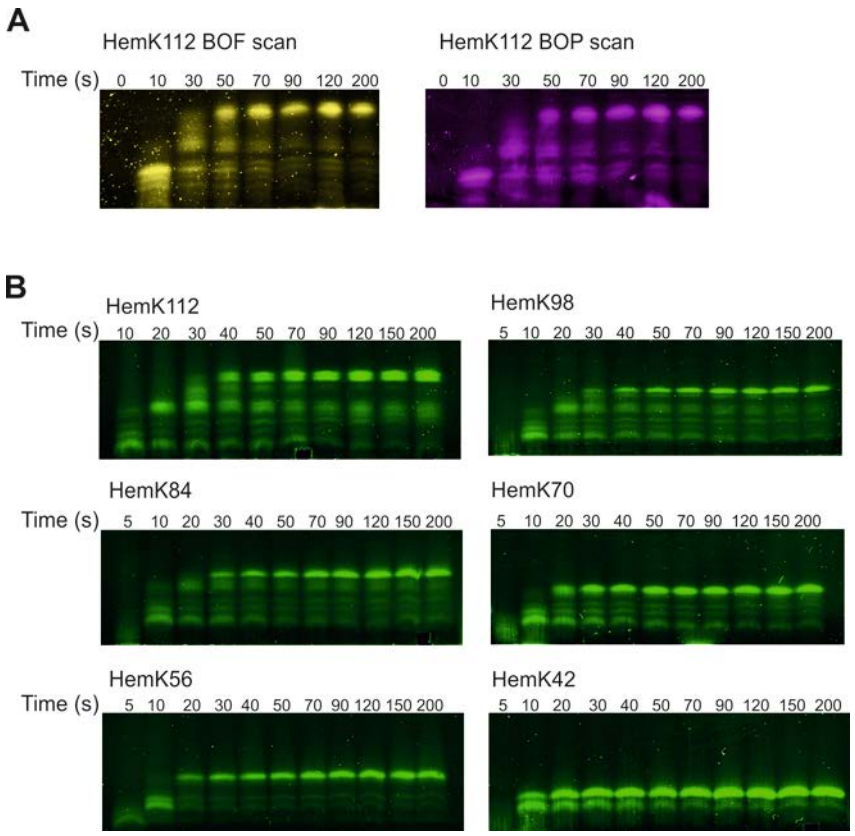

fig. S5.

Related to Fig. 2. Kinetics of translation monitored by SDS-PAGE.

(A) Translation products visualized by scanning at the excitation wavelength of BOF (BOF scan, pseudo-color yellow) or of BOP (BOP scan, pseudo-color magenta), showing that both reporter dyes were efficiently incorporated into peptides during translation of HemK112 mRNA.

(B) Time courses of translation of HemK constructs of different lengths. BOF fluorescence is shown.

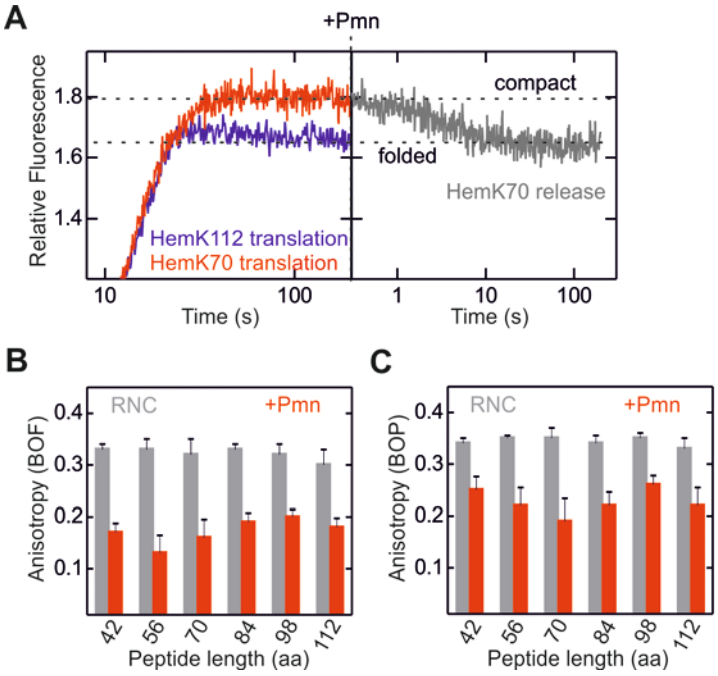

fig. S6.

Related to Fig. 2. Transition from the compact to native-like fold of HemK70 upon release of the nascent chain with puromycin.

(A) FRET change upon the release of HemK70 (red) from the ribosome by puromycin treatment, FRET decreases (gray) to the same level as reached during translation of HemK112 (blue).

(B) Anisotropy of BOF-labeled polypeptide chains of different lengths. Ribosome-nascent chains (gray) or polypeptides released into solution by puromycin (red).

(C) Same as in (B) for BOP at position 34 of the polypeptide chain. High anisotropy of ribosome-bound chains reflects the low degree of conformational freedom when bound to the ribosome.

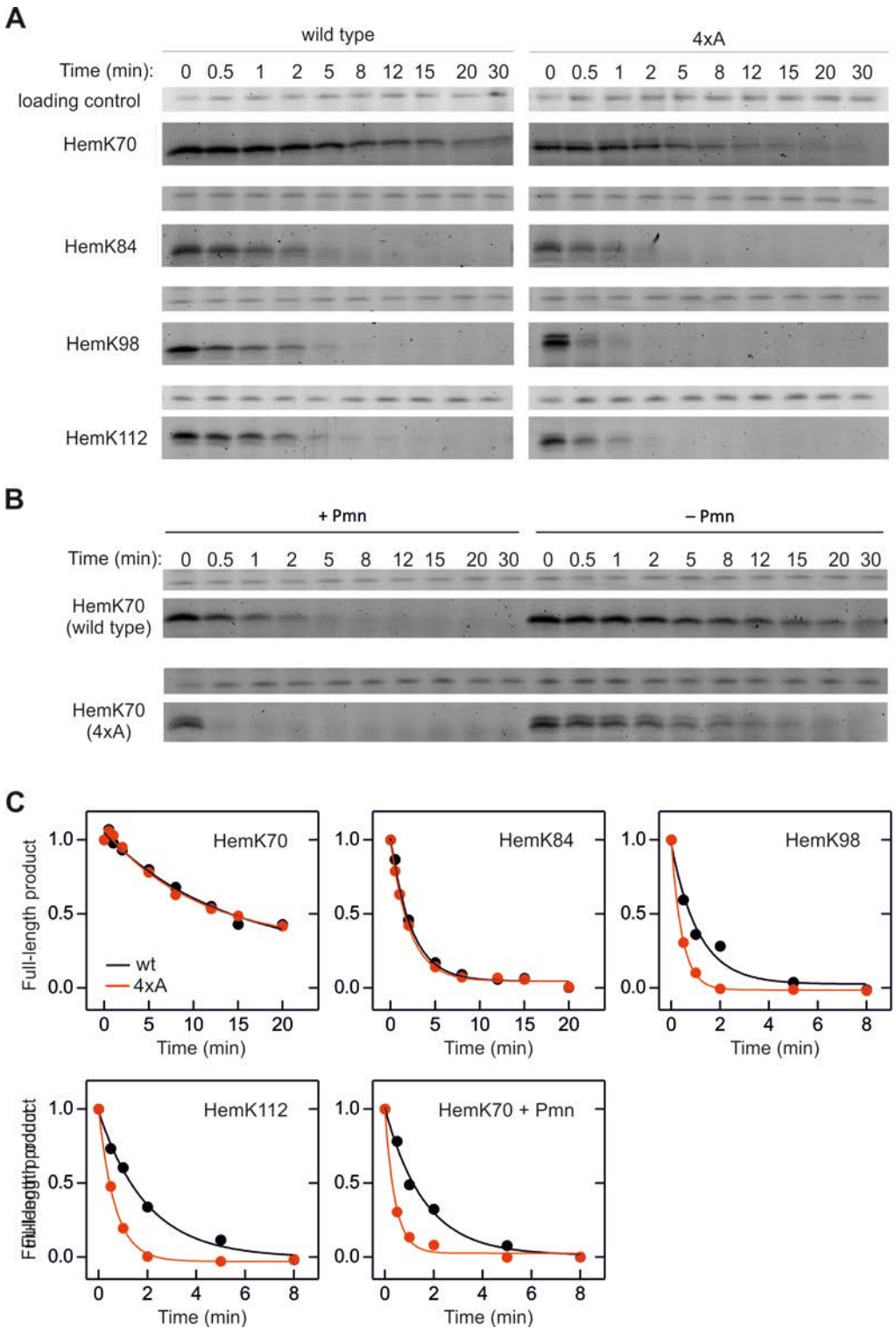

fig. S7.

Related to Fig. 3. Time-resolved proteolysis of wt and 4xA HemK NTD constructs.

(A) SDS-PAGE of protease digestion products. Loading controls are taken from the constant band visible in the BOP channel and representing the minute amount of residual undigested

BOP-Lys-tRNA. The same amounts of BOP-Lys-tRNA were used in all experiments, and all samples were treated in the same way; therefore the amount of undigested BOP-Lys-tRNA should be identical in all samples.

(B) Protease digestion of HemK70 (wt and 4xA) released from the ribosome by puromycin treatment (+ puromycin) or attached to the ribosome (no puromycin).

(C) Quantification of the time courses of protease digestion for wt (black) and 4xA (red) constructs. Smooth lines represent single-exponential fits used to calculate τ_{wt}/τ_{4xA} (Fig. 3C).

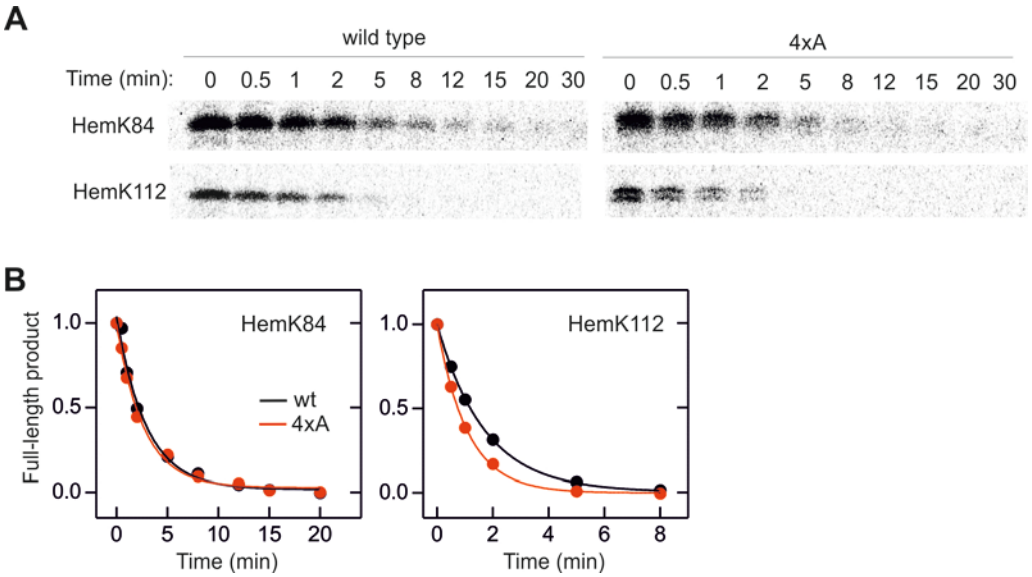

fig S8.

Related to Fig. 3. Time-resolved proteolysis of the wt and 4xA HemK NTD constructs not labeled with fluorescence dyes.

(A) SDS-PAGE of protease digestion products labeled with [^{35}S]Met visualized by radioactive scanning. Same amounts of ribosomes were loaded in every lane.

(B) Quantification of the time courses of protease digestion for wt (black) and 4xA (red) constructs. Smooth lines represent single-exponential fits.

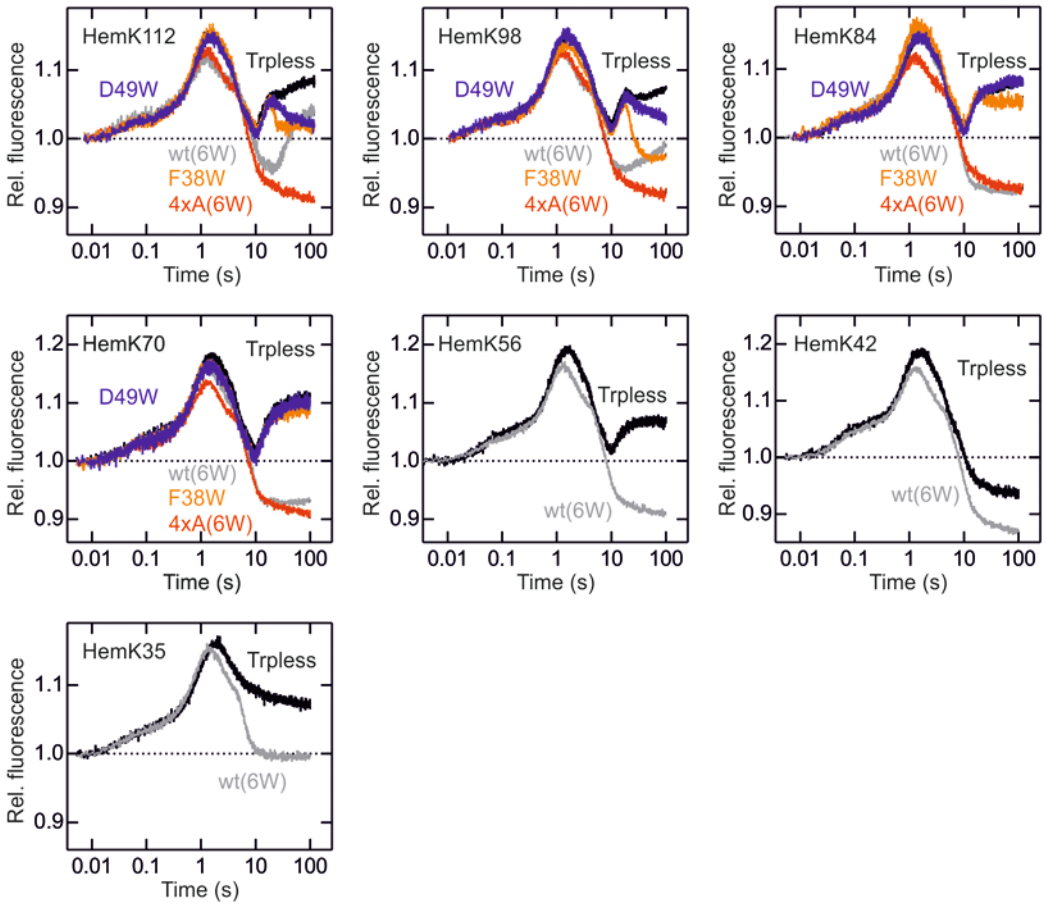

fig. S9.

Related to Fig. 4. Transient PET changes for various HemK constructs of different lengths. Trp-less denotes HemK without Trp residues which was used as a background signal reflecting changes of BOF-Met fluorescence during movement through the peptide exit tunnel. The values measured with Trp-less HemK were subtracted from all other time courses to yield the corrected PET time courses depicted in Fig. 4B,D.

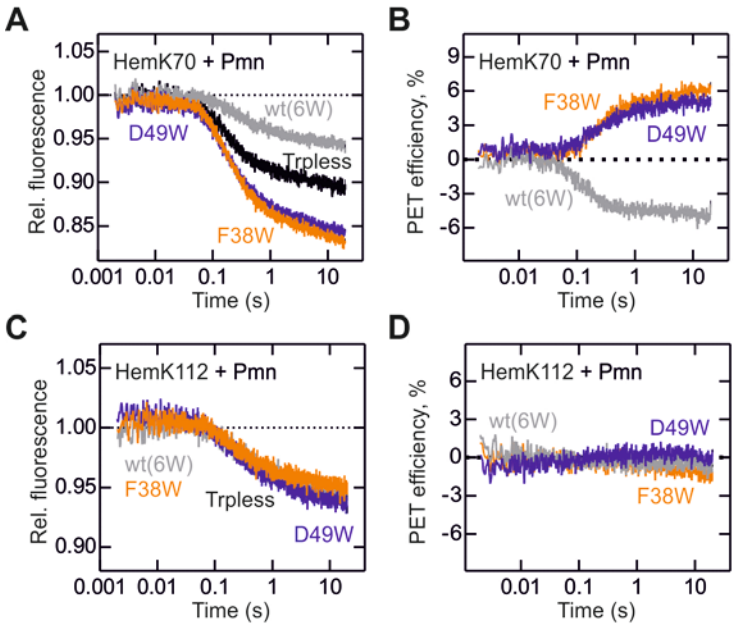

fig S10.

Related to Fig. 4. Rearrangements in HemK70 and 112 upon release from the ribosome.

(A) Fluorescence changes of N-terminally BOF-labeled HemK70 following the release of nascent chains from the ribosome after puromycin treatment.

(B) PET change, calculated by subtraction of the Trpless control from the respective trace containing Trp at the indicated position. The direction of the PET change (increase for Trp at positon 38 (orange) and 49 (blue), decrease for Trp at position 6 (grey)) and the magnitude of the reaction is consistent with the change observed when the ribosome-bound nascent polypeptide chains were extended from 70 to 112 (Fig. 4C,E), indicating a similar conformation of the NTD when extruded from the tunnel but attached to the ribosome and after folding in solution.

(C) Fluorescence changes of BOF-labeled HemK112 after release from the ribosome with puromycin; Trp control is not visible as it is identical to the other three traces.

(D) PET changes calculated as in (B); no further PET change is observed after HemK112 was released from the ribosome, indicating that the ribosome-bound HemK NTD is in a native-like fold that does not rearrange further after release from the ribosome.

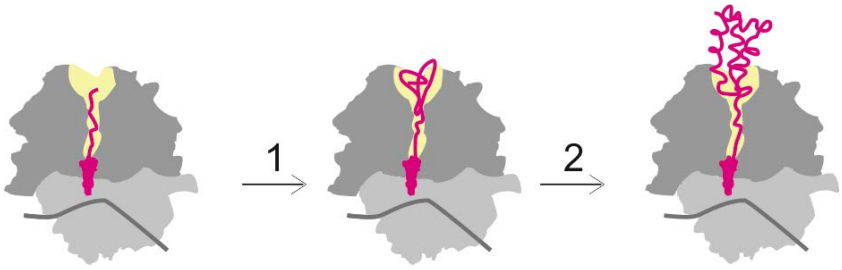

fig S11.

Related to Figs. 2-4. Schematics of co-translational folding of the HemK NTD.

Small and large ribosomal subunits are shown in light and dark grey, respectively, polypeptide exit tunnel is depicted in yellow with a more spacious area indicating the vestibule. mRNA is in very dark gray, tRNA and the nascent peptide are shown in magenta. Step 1, formation of a compact folding state within the ribosome exit tunnel upon incorporation of the N-terminal 56-70 amino acids. Step 2, folding into the native-like structure upon emergence of the entire NTD from the peptide exit tunnel.

Table S1.

Related to Fig. 1. Summary of thermodynamic and kinetic parameters of HemK NTD.

Method	m_G (kJ/mol M)	m_f (kJ/mol M)	m_U (kJ/mol M)	$\Delta G(0)$ kJ/mol	[Urea $_{1/2}$] (M)	β^{TS}	k_f (s^{-1})	k_{uf} (s^{-1})	τ_0 (µs)
Equilibrium unfolding	4.80 (0.09)	-	-	20.78 (0.38)	4.33 (0.12)	-	-	-	-
Kinetic data	4.76 (0.09)	3.22 (0.07)	1.54 (0.03)	19.50 (0.40)	-	0.68	5137 (366)	1.97 (0.15)	195 (6)

The equilibrium data are from the least-squares fit of eq. 3 to the experimental data in Fig. S2, panel A. The kinetic data are from the least-squares fit of eq. 5 to the experimental data in Fig. S2, panel D. $\Delta G(0)$ is the free energy of folding in the absence of denaturant. The kinetic value was calculated from the extrapolated folding and unfolding rates in the absence of denaturant ($\Delta G(0) = -RT \cdot \ln(k_f/k_{uf})$). [Urea ½] = $\Delta G(0)/m_G$ is the urea concentration at which $\Delta G=0$ (midpoint of unfolding transition). m_G is the cooperativity parameter of unfolding. Its magnitude is proportional to the change in solvent-exposed surface area upon folding. The kinetic m_G-value was calculated from the slopes of the dependence of the folding (m_f) and unfolding rate constants (m_u) on urea ($m_G = mf + m_u$). In analogy to m_G, m_f and m_u are proportional to the change in solvent-exposed area between the unfolded state and the transition state, and between the transition state and the native state, respectively. β^{TS} (also known as the Tanford β-value) is a dimensionless parameter that describes the location of the folding transition state (TS) along the reaction coordinate of folding (0-1). It is calculated from $\beta^T = m_f/(m_f + m_u)$. The calculated $\beta^{TS\ f}$ for HemK NTD indicates that about 70 % of the native state contacts are already formed in the folding transition state, a value that agrees well with the empirical 70% rule from numerous other folding studies.

References

1. Y. Han, A. David, B. Liu, J. G. Magadán, J. R. Bennink, J. W. Yewdell, S. B. Qian, Monitoring cotranslational protein folding in mammalian cells at codon resolution. *Proc. Natl. Acad. Sci. U.S.A.* **109**, 12467–12472 (2012). Medline doi:10.1073/pnas.1208138109

2. S. T. Hsu, P. Fucini, L. D. Cabrita, H. Launay, C. M. Dobson, J. Christodoulou, Structure and dynamics of a ribosome-bound nascent chain by NMR spectroscopy. *Proc. Natl. Acad. Sci. U.S.A.* **104**, 16516–16521 (2007). Medline doi:10.1073/pnas.0704664104

3. C. Eichmann, S. Preissler, R. Riek, E. Deuerling, Cotranslational structure acquisition of nascent polypeptides monitored by NMR spectroscopy. *Proc. Natl. Acad. Sci. U.S.A.* **107**, 9111–9116 (2010). Medline doi:10.1073/pnas.0914300107

4. C. A. Woolhead, P. J. McCormick, A. E. Johnson, Nascent membrane and secretory proteins differ in FRET-detected folding far inside the ribosome and in their exposure to ribosomal proteins. *Cell* **116**, 725–736 (2004). Medline doi:10.1016/S0092-8674(04)00169-2

5. J. Lu, C. Deutsch, Folding zones inside the ribosomal exit tunnel. *Nat. Struct. Mol. Biol.* **12**, 1123–1129 (2005). Medline doi:10.1038/nsmb1021

6. S. Bhushan, M. Gartmann, M. Halic, J. P. Armache, A. Jarasch, T. Mielke, O. Berninghausen, D. N. Wilson, R. Beckmann, α-Helical nascent polypeptide chains visualized within distinct regions of the ribosomal exit tunnel. *Nat. Struct. Mol. Biol.* **17**, 313–317 (2010). Medline doi:10.1038/nsmb.1756

7. O. B. Nilsson, R. Hedman, J. Marino, S. Wickles, L. Bischoff, M. Johansson, A. Müller-Lucks, F. Trovato, J. D. Puglisi, E. P. O'Brien, R. Beckmann, G. von Heijne, Cotranslational protein folding inside the ribosome exit tunnel. *Cell Rep.* **12**, 1533–1540 (2015). Medline

8. J. Kubelka, T. K. Chiu, D. R. Davies, W. A. Eaton, J. Hofrichter, Sub-microsecond protein folding. *J. Mol. Biol.* **359**, 546–553 (2006). Medline doi:10.1016/j.jmb.2006.03.034

9. C. M. Kaiser, D. H. Goldman, J. D. Chodera, I. Tinoco Jr., C. Bustamante, The ribosome modulates nascent protein folding. *Science* **334**, 1723–1727 (2011). Medline doi:10.1126/science.1209740

10. Y. E. Kim, M. S. Hipp, A. Bracher, M. Hayer-Hartl, F. U. Hartl, Molecular chaperone functions in protein folding and proteostasis. *Annu. Rev. Biochem.* **82**, 323–355 (2013). Medline doi:10.1146/annurev-biochem-060208-092442

11. F. Gloge, A. H. Becker, G. Kramer, B. Bukau, Co-translational mechanisms of protein maturation. *Curr. Opin. Struct. Biol.* **24**, 24–33 (2014). Medline doi:10.1016/j.sbi.2013.11.004

12. S. Pechmann, F. Willmund, J. Frydman, The ribosome as a hub for protein quality control. *Mol. Cell* **49**, 411–421 (2013). Medline doi:10.1016/j.molcel.2013.01.020

13. A. A. Komar, A pause for thought along the co-translational folding pathway. *Trends Biochem. Sci.* **34**, 16–24 (2009). Medline doi:10.1016/j.tibs.2008.10.002

14. G. Zhang, Z. Ignatova, Folding at the birth of the nascent chain: Coordinating translation with co-translational folding. *Curr. Opin. Struct. Biol.* **21**, 25–31 (2011). Medline doi:10.1016/j.sbi.2010.10.008

15. J. Mittelstaet, A. L. Konevega, M. V. Rodnina, A kinetic safety gate controlling the delivery of unnatural amino acids to the ribosome. *J. Am. Chem. Soc.* **135**, 17031–17038 (2013). Medline doi:10.1021/ja407511q

16. Z. Yang, L. Shipman, M. Zhang, B. P. Anton, R. J. Roberts, X. Cheng, Structural characterization and comparative phylogenetic analysis of *Escherichia coli* HemK, a protein (N5)-glutamine methyltransferase. *J. Mol. Biol.* **340**, 695–706 (2004). Medline doi:10.1016/j.jmb.2004.05.019

17. H. Chen, S. S. Ahsan, M. B. Santiago-Berrios, H. D. Abruña, W. W. Webb, Mechanisms of quenching of Alexa fluorophores by natural amino acids. *J. Am. Chem. Soc.* **132**, 7244–7245 (2010). Medline doi:10.1021/ja100500k

18. N. Marmé, J. P. Knemeyer, M. Sauer, J. Wolfrum, Inter- and intramolecular fluorescence quenching of organic dyes by tryptophan. *Bioconjug. Chem.* **14**, 1133–1139 (2003). Medline doi:10.1021/bc0341324

19. B. Keil, *Specificity of Proteolysis* (Springer-Verlag, Berlin, 1992).

20. S. Doose, H. Neuweiler, M. Sauer, Fluorescence quenching by photoinduced electron transfer: A reporter for conformational dynamics of macromolecules. *ChemPhysChem* **10**, 1389–1398 (2009). Medline doi:10.1002/cphc.200900238

21. E. P. O'Brien, J. Christodoulou, M. Vendruscolo, C. M. Dobson, New scenarios of protein folding can occur on the ribosome. *J. Am. Chem. Soc.* **133**, 513–526 (2011). Medline doi:10.1021/ja107863z

22. A. Kosolapov, C. Deutsch, Tertiary interactions within the ribosomal exit tunnel. *Nat. Struct. Mol. Biol.* **16**, 405–411 (2009). Medline doi:10.1038/nsmb.1571

23. I. M. Sander, J. L. Chaney, P. L. Clark, Expanding Anfinsen's principle: Contributions of synonymous codon selection to rational protein design. *J. Am. Chem. Soc.* **136**, 858–861 (2014). Medline doi:10.1021/ja411302m

24. L. K. Doerfel, I. Wohlgemuth, C. Kothe, F. Peske, H. Urlaub, M. V. Rodnina, EF-P is essential for rapid synthesis of proteins containing consecutive proline residues. *Science* **339**, 85–88 (2013). Medline doi:10.1126/science.1229017

25. P. Milon, A. L. Konevega, F. Peske, A. Fabbretti, C. O. Gualerzi, M. V. Rodnina, Transient kinetics, fluorescence, and FRET in studies of initiation of translation in bacteria. *Methods Enzymol.* **430**, 1–30 (2007). Medline doi:10.1016/S0076-6879(07)30001-3

26. J. Mittelstaet, A. L. Konevega, M. V. Rodnina, A kinetic safety gate controlling the delivery of unnatural amino acids to the ribosome. *J. Am. Chem. Soc.* **135**, 17031–17038 (2013). Medline doi:10.1021/ja407511q

27. M. V. Rodnina, W. Wintermeyer, GTP consumption of elongation factor Tu during translation of heteropolymeric mRNAs. *Proc. Natl. Acad. Sci. U.S.A.* **92**, 1945–1949 (1995). Medline doi:10.1073/pnas.92.6.1945

28. W. Holtkamp, C. E. Cunha, F. Peske, A. L. Konevega, W. Wintermeyer, M. V. Rodnina, GTP hydrolysis by EF-G synchronizes tRNA movement on small and large ribosomal subunits. *EMBO J.* **33**, 1073–1085 (2014). Medline doi:10.1002/embj.201387465